

On the calculation of 3-D apparent resistivity responses with conductive plates

César Barajas¹ and Carlos Flores

Depto. de Geofísica Aplicada, CICESE., Ensenada, Baja California, México.

¹ *Presently at: Institut für Geophysik, Christian-Albrechts-Universität Kiel, Fed. Rep. of Germany*

Received: August 19, 1993; accepted: December 2, 1993.

RESUMEN

Se aplica una técnica de ecuación integral para modelar la respuesta tri-dimensional de resistividad aparente de un conjunto de placas conductoras en una tierra homogénea o estratificada. En la implementación del algoritmo la ecuación integral de Fredholm de segunda clase se transforma en una ecuación matricial, la cual se resuelve para las componentes de dipolos de corriente distribuidos sobre los planos de las placas. La resistividad aparente en la superficie se obtiene a partir de los potenciales secundarios producidos por los dipolos de corriente.

Se examina la exactitud de las respuestas calculadas con cinco modelos de prueba. Puesto que de estos modelos ninguno tiene solución analítica que pudiera considerarse como una solución verdadera, la exactitud está definida con respecto a resultados numéricos de convergencia o con la comparación con otras respuestas numéricas independientes publicadas con anterioridad. En los tres primeros modelos se consideran heterogeneidades de una sola placa con diferentes inclinaciones (horizontal, vertical, y buzando a 45 grados). En los últimos dos casos se prueba la aproximación con placas de cuerpos sólidos conductores, considerando en uno de estos modelos un medio huésped estratificado. Las respuestas se comparan con seis diferentes soluciones independientes reportadas en la literatura. En general los ajustes entre las respuestas son buenos, pero no óptimos. La técnica de densidad superficial de carga parece mostrar un mejor comportamiento de convergencia que el de nuestro método de dipolos de corriente y la simulación de cuerpos sólidos muestra algunas discrepancias relativamente grandes (menores del 20%) en las resistividades aparentes localizadas arriba de las placas. A pesar de estas limitaciones, el método de placas promete ser una herramienta útil en la interpretación de levantamientos de resistividad en estudios geotérmicos, mineros y geohidrológicos, donde pueden existir varios conductores.

PALABRAS CLAVE: Modelado en resistividad, placas conductoras, análisis de exactitud.

ABSTRACT

An integral equation technique is applied for modeling the three-dimensional apparent resistivity response of a set of conductive plates immersed in a homogeneous or stratified earth. In implementing the algorithm, the Fredholm integral equation of the second kind is transformed into a matrix equation and solved for the components of distributed current dipoles lying on the planes of the plates. The apparent resistivity at the earth's surface is obtained from the secondary potentials produced by the current dipoles.

The accuracy of the computed responses is examined in five test models. Because there is not any analytical solution for these models which could be considered as a true solution, the accuracy is defined in terms of converging numerical results or by comparison with other previously published independent numerical responses. In the first three models single-plate inhomogeneities are considered with different inclinations (horizontal, vertical, and dipping at 45 degrees). In the last two cases the approximation of solid conductive bodies with plates is tested, considering in one of these models a layered host medium. The responses are compared with six different independent solutions reported in the literature. The overall agreement between the responses is good but not optimum. The surface charge density approach seems to show a better converging behavior than our current dipole scheme and the simulation of solid bodies shows some relatively large discrepancies (less than 20%) in the apparent resistivities right over the plates. Despite these limitations, the multiplate technique promises to be a useful tool in the interpretation of resistivity surveys in geothermal, mineral, and groundwater environments where multiple conductors may coexist.

KEY WORDS: Resistivity modeling, conductive plates, accuracy analysis.

INTRODUCTION

The resistivity method has been extensively utilized in the exploration of groundwater, mineral, and geothermal resources. In many of these applications one- or two-dimensional interpretations may yield erroneous results when the underground resistivity distribution is three-dimensional (3-D). The approach most often used in these cases is numerical modeling of 3-D structures employing one of the following techniques: finite differences (Dey and Morrison, 1979), finite element (Pridmore *et al.*, 1981), or integral equation (e.g. Dieter *et al.*, 1969; Hohmann, 1975; Okabe, 1981; Das and Parasnis, 1987). In the first two techniques arbitrary resistivity distributions

can be modeled, but they demand very large computer resources as the whole earth is discretized. The integral equation method, although generally limited to confined bodies, has the advantage of requiring computer resources more easily available as only the anomalous bodies are discretized.

Nabighian *et al.* (1984) and Cheesman and Edwards (1989) proposed an integral equation approach to calculate the magnetometric resistivity response of a set of conductive plates in a homogeneous half-space. In this paper, we use this technique to compute the apparent resistivity response of the same model but extending it to consider a two-layered earth host medium. In complex geologic envi-

ronments often encountered in geothermal and mineral prospecting the presence of several conductive inhomogeneities is not unusual. These anomalous zones can be either the actual objects of search or zones that are not of economic interest but that have the undesirable effect of reducing the detectability of the targets, such as conductive paleochannels, thickness variations in the overburden layer, or zones of hydrothermal alteration. The multiple plate model represents a promising strategy for the analysis and modeling of these field situations.

In this work we analyze the effect of several discretization factors on the apparent resistivity response computed with the plate model; to our knowledge, this has not been done before. It is important to understand the limitations of different models if this method is to be applied to the interpretation of actual field data. We propose a weighted discretization to avoid unnecessary gridding in the deep portions of the plate and we show that this model can simulate sheet-like inhomogeneities and approximates the response of solid bodies if two or more plates are used.

NUMERICAL SOLUTION OF THE INTEGRAL EQUATION

Consider the model shown in Figure 1a consisting of a set of dipping conductive plates embedded in a layered host medium. At the surface of the half-space there is a current source and a current sink electrodes denoted by C_1 and C_2 , respectively. The problem is stated as the calculation of the potential at the surface point P when a steady current I flows between the current electrodes. This potential is the sum of two contributions: a normal or primary part due to the layered half-space and an anomalous or secondary part due to the perturbation produced by the conductive plates. To calculate the anomalous potential the plates are replaced by a distribution of current dipoles on the planes of the plates. The current dipoles are obtained from a Fredholm integral equation of the second kind derived from the boundary condition for the continuity of the electric field tangential to the plates. Nabighian *et al.* (1984) and Cheesman and Edwards (1989) presented detailed derivations and discussions of the physics involved in this approach. To illustrate this integral equation technique and to introduce the different model parameters we will briefly present the numerical solution for a vertical plate. The modifications to this scheme brought by the more complicated model of a set of dipping plates in a layered earth will be considered as extensions of the simpler case.

For a single vertical plate in the plane $x = 0$ immersed in a homogeneous half-space of resistivity ρ_h , the discretized integral equations for the components of the surface current k_y and k_z , have the form (Nabighian *et al.*, 1984)

$$\frac{k_y(i)}{S(i)} = \frac{\rho_h}{4\pi} \sum_{j=1}^N [k_y(j)G_{yy}(i, j) + k_z(j)G_{yz}(i, j)] + E_y^{imp}(i) + [\text{image terms}], \quad (1)$$

and

$$\frac{k_z(i)}{S(i)} = \frac{\rho_h}{4\pi} \sum_{j=1}^N [k_y(j)G_{zy}(i, j) + k_z(j)G_{zz}(i, j)] + E_z^{imp}(i) + [\text{image terms}]$$

These expressions are obtained by dividing the plate of Figure 1b into N rectangular cells. The coordinates of the center of a given field cell, defined by the index i , are (y_i, z_i) . Those of a source cell, denoted by the index j , are (y_j, z_j) . $S(i)$ specifies the conductance of the i th cell. Over the surface of a given cell of area $A = \Delta y \Delta z$ the two components of the surface current, k_y and k_z , are assumed to be constant. The Green's functions G are given by

$$G_{yy}(i, j) = - \frac{(y_i - y')(z_i - z')}{\left[(x_2 - x_1)^2 + (y_i - y')^2 \right] R} \Big|_{z'=z(j)-\Delta z(j)/2}^{z(j)+\Delta z(j)/2} \Big|_{y'=z(j)-\Delta y(j)/2}^{y(j)+\Delta y(j)/2}$$

$$G_{yz}(i, j) = G_{zy}(i, j) = \frac{1}{R} \parallel;$$

$$G_{zz}(i, j) = - \frac{(y_i - y')(z_i - z')}{\left[(x_2 - x_1)^2 + (z_i - z')^2 \right] R} \parallel,$$

where $R^2 = (x_2 - x_1)^2 + (y_i - y')^2 + (z_i - z')^2$. The distance $x_2 - x_1$, which is zero for the single vertical plate, reflect the kind of modifications that have to be made to the G functions for computing interactions between two parallel plates of x -coordinates x_1 and x_2 , respectively.

The first and second subscripts of the Green's functions in (2) stand for the component of the electric field and the component of the electric dipole source, respectively, e.g. $G_{yz}(i, j)$ is the y -component of the electric field at the center of the i th test cell produced by the z -directed current dipole uniformly distributed over the area of the j th source cell. The current dipole moments, m_y and m_z , are the surface currents, k_y and k_z , multiplied by the cell area. Expressions (2) are derived by integrating over a rectangular cell the fields produced by point current dipoles.

The terms E_y^{imp} and E_z^{imp} in (1) are the y - and z -components of the impressed electric field at the center of the i th cell, i.e. the tangential component to the plate of the primary electric field produced by the pair of current electrodes. They are given by

$$E_y^{imp} = \frac{\rho_h}{2\pi} \left[\frac{y_i - y_{c1}}{r_{c1}^3} - \frac{y_i - y_{c2}}{r_{c2}^3} \right], \quad (3)$$

$$E_z^{imp} = \frac{\rho_h}{2\pi} \left[\frac{z_i}{r_{c1}^3} - \frac{z_i}{r_{c2}^3} \right],$$

with $r_{c1}^2 = (x_i - x_{c1})^2 + (y_i - y_{c1})^2 + z_i^2$

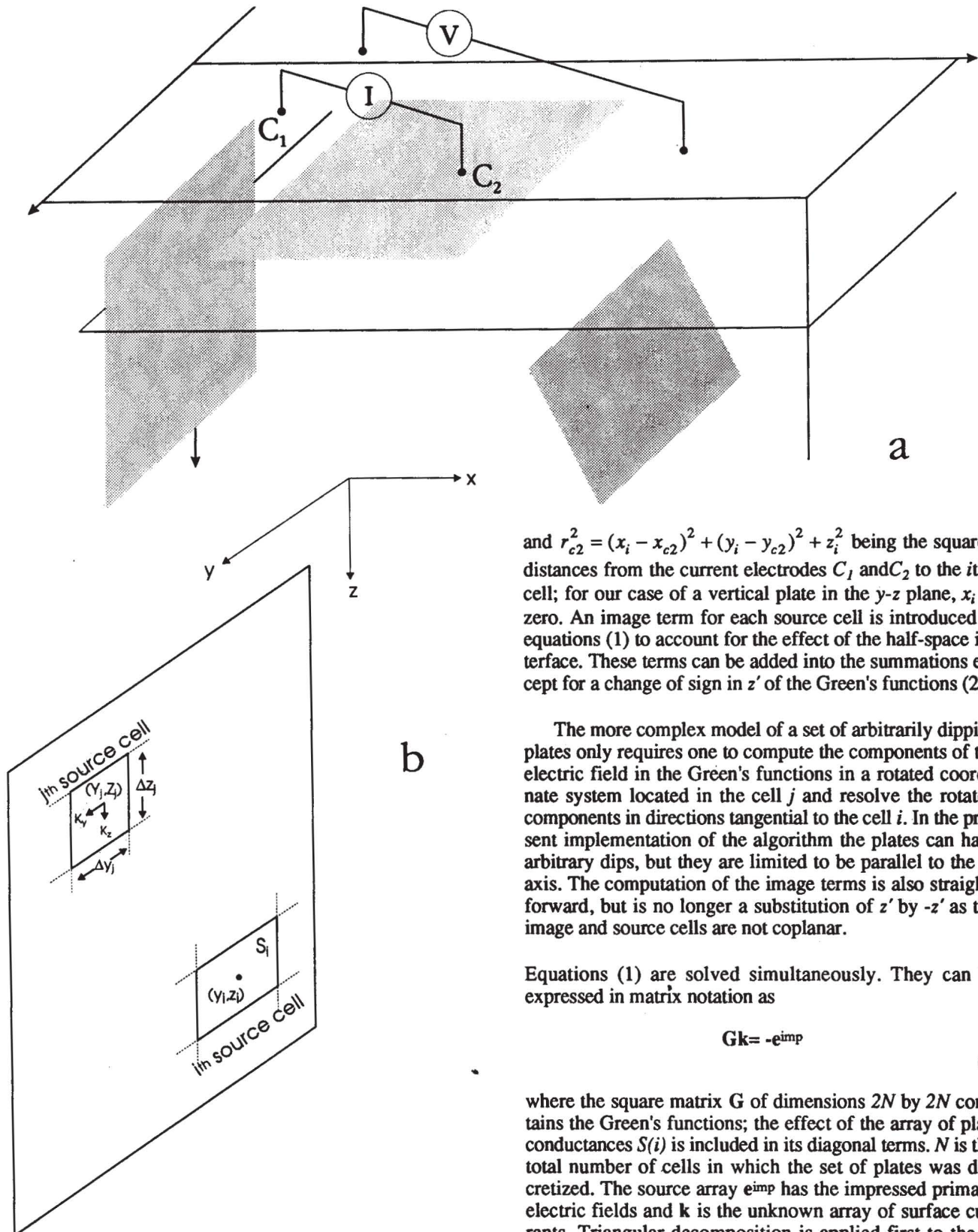


Fig. 1. a) The multiple plate model in a layered host excited by a pair of point current electrodes at the surface. b) A single vertical plate in the plane $x=0$ showing the source and field cells (k_y and k_z are the components of the surface current).

and $r_{c2}^2 = (x_i - x_{c2})^2 + (y_i - y_{c2})^2 + z_i^2$ being the squared distances from the current electrodes C_1 and C_2 to the i th cell; for our case of a vertical plate in the y - z plane, x_i is zero. An image term for each source cell is introduced in equations (1) to account for the effect of the half-space interface. These terms can be added into the summations except for a change of sign in z' of the Green's functions (2).

The more complex model of a set of arbitrarily dipping plates only requires one to compute the components of the electric field in the Green's functions in a rotated coordinate system located in the cell j and resolve the rotated components in directions tangential to the cell i . In the present implementation of the algorithm the plates can have arbitrary dips, but they are limited to be parallel to the y -axis. The computation of the image terms is also straightforward, but is no longer a substitution of z' by $-z'$ as the image and source cells are not coplanar.

Equations (1) are solved simultaneously. They can be expressed in matrix notation as

$$\mathbf{G}\mathbf{k} = -\mathbf{e}^{imp} \quad (4)$$

where the square matrix \mathbf{G} of dimensions $2N$ by $2N$ contains the Green's functions; the effect of the array of plate conductances $S(i)$ is included in its diagonal terms. N is the total number of cells in which the set of plates was discretized. The source array \mathbf{e}^{imp} has the impressed primary electric fields and \mathbf{k} is the unknown array of surface currents. Triangular decomposition is applied first to the \mathbf{G} matrix followed by forward and backward substitutions to determine the $2N$ unknown surface currents. For a given model this computing procedure has the advantage of performing only once the triangular decomposition as the

variable impressed fields associated with a mobile electrode array are accounted by the forward and backward substitution processes. The moments of the current dipoles, m_y and m_z are obtained from the corresponding surface currents by multiplying them by the cell area A .

Having found the moments of the distributed current dipoles in each cell, the total potential at any point on the surface of the Earth is calculated from

$$V^{\text{tot}}(i) = V^{\text{pri}}(i) + \frac{\rho_h}{4\pi} \sum_{j=1}^N [m_y(j)V_y(i,j) + m_z(j)V_z(i,j)] / A(j) + [\text{image terms}] \quad (5)$$

where V^{pri} is the primary potential produced by the pair of current electrodes at the surface, and i stands now for the coordinates of the observation point. The second and third terms on the right hand side of equation (5), together with the image terms, express the secondary potential resulting from the inhomogeneity. The V_y and V_z are the potentials produced by y - and z - directed unit current dipoles uniformly distributed over the area of a rectangular cell and are derived by integrating twice the potentials due to point current dipoles. They are given by

$$V_y(i,j) = -1 \ln \left[(z_i - z') + r \right] \Big|_{z'=z(j)-\Delta z(j)/2}^{z(j)+\Delta z(j)/2} \Big|_{y'=y(j)-\Delta y(j)/2}^{y(j)+\Delta y(j)/2} \quad (6)$$

and

$$V_z(i,j) = -1 \ln \left[(y_i - y') + r \right]$$

where, $r^2 = (x_i - x')^2 + (y_i - y')^2 + (z_i - z')^2$, with $x' = 0$ for our single vertical plate.

Finally, the apparent resistivities are computed from the potentials using

$$\rho_a = 2\pi K (V_M^{\text{tot}} - V_N^{\text{tot}}) / I$$

where V_M^{tot} and V_N^{tot} are the total potentials at the potential electrodes M and N , and K is the standard geometric factor involving the distances between the two current and two potential electrodes.

For a layered earth an infinite sum of image terms is required for each element of the matrix G , the impressed fields, and both the primary and secondary potentials. A derivation of the expansions into images of the potentials in a two-layered half-space is detailed in the Appendix. There is no theoretical limitation for the extension to earths of more than two layers, but the handling of the images is too cumbersome. For these stratified hosts the digital filtering technique (Das and Parasnis, 1987) is recommended. For the two-layered case the image and filtering techniques are equivalent in terms of computing time.

NUMERICAL TESTS

Different numerical aspects of the use of the plate model are illustrated in the following five test cases. In the first two cases the effects on the accuracy of the cell discretization are addressed. The other three cases consider comparisons with several independent numerical solutions reported in the literature.

The Horizontal Plate

Figure 2a shows the model and electrode array considered in this test. The model consists of a 100 by 100 m horizontal plate of conductance 100 S embedded in a homogeneous half-space of 100 $\Omega \cdot m$ at a depth of 25 m. To calculate the apparent resistivities a pole-pole array was used keeping the current electrode C_1 fixed at the origin of coordinates and moving the potential electrode P_1 along the diagonal profile shown in the figure. The other two electrodes C_2 and P_2 were located at a large distance away to simulate the electrodes-at-infinity of this array. The same apparent resistivities are obtained in this and the following tests if the dimensions of the model and the lengths of the electrode array are scaled.

We divided the plate into three different homogeneous grids of 4x4, 8x8, and 15x15 ($N = 16, 64, \text{ and } 225$ square cells). The corresponding calculated apparent resistivity profiles are displayed in Figure 2b. Notice that convergence is practically achieved for the 15x15 grid. As an analytical solution to this problem does not exist, we will assume the apparent resistivities obtained from this fine grid are "true" values in order to estimate accuracy errors of grosser grids. Figure 2c shows the absolute percentage errors of the 4x4 and 8x8 grids with respect to the 15x15 grid. A parameter that describes the discretization into cells is the ratio Δ/d where Δ is the side length of a square cell and d is its depth (25 m for this model). It is clear that Δ alone is not sufficient to describe the cell discretization. A given plate will require smaller cells as its depth decreases to reach a nominal accuracy. The 4x4 and 8x8 grids have Δ/d ratios of 1.0 and 0.5, respectively, with associated maximum errors of 2.7 % and 0.9 % (Figure 2c). This numerical test reflects a general result obtained with other models (Barajas, 1989), that is, if nominal accuracies in the apparent resistivity response of a single horizontal plate of the order of 5 % or 1 % are desired, Δ/d ratios of 1.0 or 0.5 are required in the cell discretization.

A conductive inhomogeneity within the earth channels the current flow set up by the electrodes at the surface (Nabighian *et al.*, 1984). This channeling ability depends both on the geometry of the body and the electrode array, and on the resistivity contrast between the inhomogeneity and the host medium. For a square plate of size L , conductance S , embedded in a host medium of resistivity ρ_h and excited by a homogeneous electric field, Nabighian *et al.* (1984) defined a current channeling number α given by $\rho_h S/L$. The ratio of the current channeled in the plate to the total current flowing in its vicinity, denoted by Cheesman and Edwards (1989) as the relative effect, is of the order of

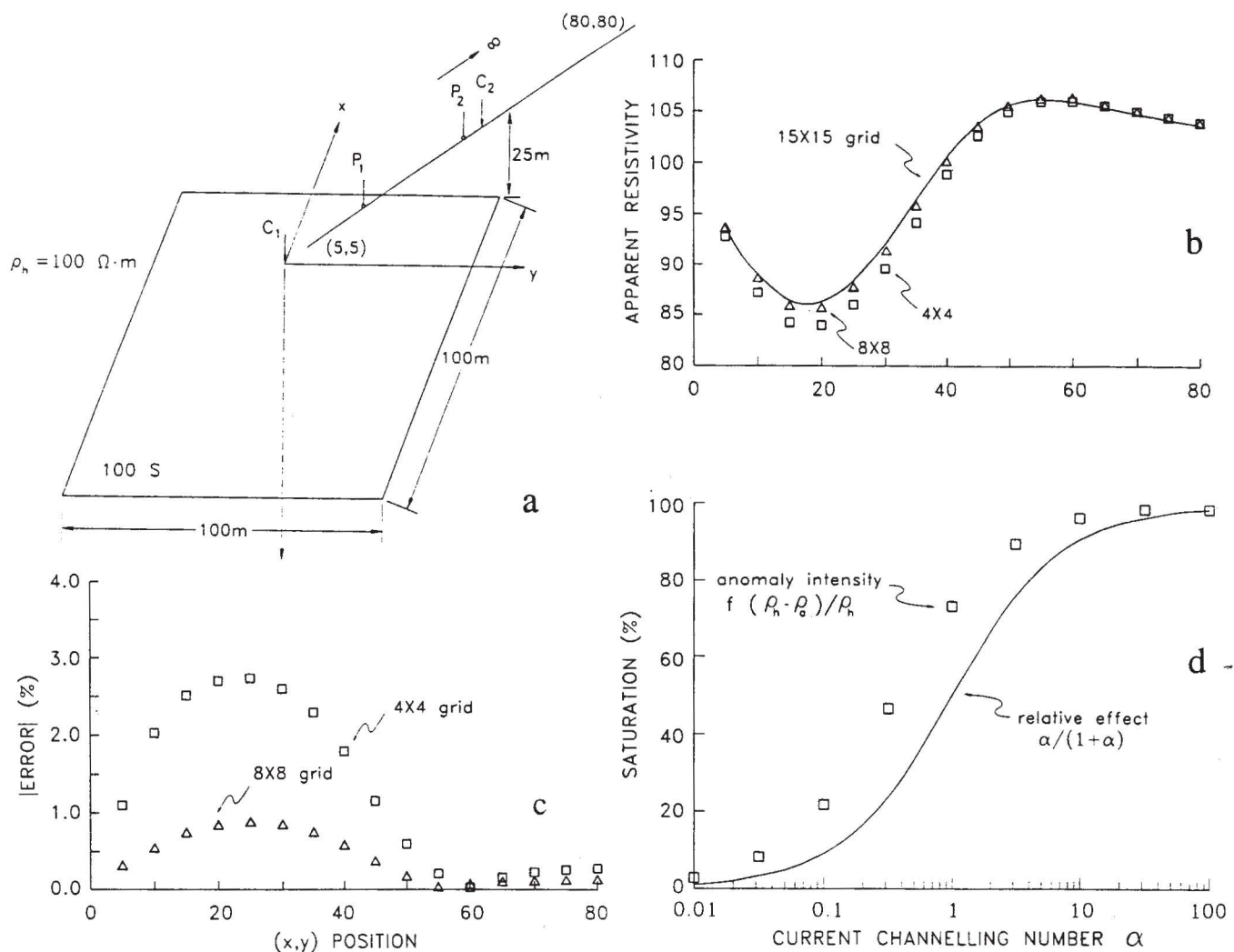


Fig. 2. a) Geometric configuration of the horizontal plate model and location of the pole-pole profile. b) Apparent resistivity re-sults for three different homogeneous discretizations. c) Absolute errors (in percentage) of the 4x4 and 8x8 grids with respect to the 15x15 grid. d) Current saturation for the horizontal plate (see text for details).

$\alpha/(1+\alpha)$. Figure 2d displays the relative effect (expressed as a percentage) as a function of the current channelling number α . The anomaly intensity can be expressed by the function $f(\rho_h \cdot \rho_a) / \rho_h$, where ρ_a is the calculated apparent resistivity at the point (20, 20) and f is a normalizing factor that accounts for the non-uniformity of the exciting field. Both functions, the relative effect and the anomaly intensity, were calculate by varying the plate conductance from 0.01 to 100 S. The important feature of Figure 2d is the similar behavior of both functions. For low conductances and therefore low channelling numbers the relative effect and the anomaly intensity are small, i.e. the plate has such a low conductance that a very small portion of the available current in the host is channeled by the plate and consequently the anomaly intensity is small. As α increases from 0.1 to 10 both the channeled current and the anomaly intensity increase linearly. At large α values current saturation occurs and the anomaly reaches its maximum possible intensity, that of a perfect conductor.

For a given plate a relationship exists between the cell size and the level of current channelling. In the current

saturation regime the intensity of the anomaly is at its maximum because the current dipoles on the plate and their spatial gradients reach their maximum values. To adequately represent this strong spatial variation requires small cells, i.e. low Δ/d ratios, to reach a nominal, say 5%, accuracy level. Conversely, if the same plate is in the regime of low current channelling numbers and the same accuracy level is desired, larger cells can be used because the lateral gradients of the current dipoles are smaller. Then, by simply inspecting the current channelling number the interpreter can predict if inhomogeneity is or is not in its current saturation level, and accordingly employ small or large cells. Notice that the Δ/d accuracy criteria proposed above for the horizontal plate represented lower bounds as they were derived in the current saturation level (plate conductance of 100 S with a corresponding channelling number of 100); if the same plate is not saturated with current the same accuracy levels can be reached with larger cells.

A feature worth noticing in this test case is that both the apparent resistivity minimum (Figure 2b) and the max-

imum errors (Figure 2c) occur in the vicinity of the point with coordinates $x=25$, $y=25$ (for brevity denoted here as the ρ_a -min zone) and not in the expected region close to the current electrode C_1 at the origin of coordinates. In order to explain this feature we will use Figures 3a and 3b, which show the spatial configuration of the current dipole moments and the impressed electric fields, respectively, plotted at the center of each cell for the 15x15 grid. We are plotting only one quadrant of the plate. The other quadrants are mirror images due to the symmetry chosen for this model and its source field. The moments of the distributed current dipoles reach their maximum values in the ρ_a -min zone. Even when the secondary potential at the surface is the sum of all cell contributions, the surface points above this zone have the strongest potentials, which in turn produce the apparent resistivities most anomalous. This also explains why the largest errors occur in the same location.

Now, to explain why the strongest current dipoles occur in the ρ_a -min zone it is interesting to note that the maximum impressed electric fields also occur in this zone (Figure 3b). This is not surprising as the spatial behavior of the current dipoles is expected to be influenced by the source field. The primary electric field pattern set up by the pair of current electrodes practically has radial symmetry with respect to the electrode C_1 . The cell immediately below this electrode is perpendicular to this field and therefore has a zero impressed field, i.e. there is no tangential field to the cell. If the plate were reduced in size to this small cell its presence could not be detected with this electrode array. This point was addressed by Grant and West (1965, p. 428) when they demonstrated that a target body resembling a conductive ribbon cannot be detected at the surface if the exciting primary field is perpendicular to its plane. In contrast, the cells at the edges of the plate are more parallel to the radially directed primary field. However, the impressed fields are not the more intense here because of the decaying behavior of the electric field with distance. This explains why the maximum impressed field occurs in the ρ_a -min zone. This zone reflects a compromise between two geometric factors. First, the geometric coupling between plate and primary electric field, i.e. the impressed electric field maximizes when the plane of the plate is parallel to the primary field, and second, the decaying character of the primary field with the distance between the plate and current electrode.

The Vertical Plate

In this case the apparent resistivity response at the surface was calculated with a mobile dipole-dipole array coplanar to the plate (Figure 4), maintaining the parameters a and n fixed with values of 3 m and 2, respectively, and moving the center of the array along the y -axis. The model is a 10 by 10 m vertical plate of conductance 10 S, located at a depth of 2.5 m in a homogeneous earth of 100 $\Omega \cdot m$.

For computing efficiency the number of cells in the deeper portions of the plate can be reduced (Flores and

Edwards, 1992). In this region the primary, and consequently the impressed electric fields, have smaller magnitudes than in the shallow region (Figure 5a) because of its larger distances from the current electrodes. This in turn yields smaller current dipole moments in the deeper parts of the plate (Figure 5b). Furthermore, the deeper cells produce smaller secondary surface potentials due to their larger depths of burial. It is clear then that the shallow portions of the plate can be discretized more finely at the expense of the deep portions. Accordingly, we weighted the vertical discretization with an inverse depth law ($1/z$). This is a compromise between the first-order approximations to the decaying behavior ($1/z^2$) of the impressed electric field (equations 3) and the logarithmic character with distance of the secondary potentials (equation 6).

To illustrate the application of the weighted vertical discretization let us consider the plate of Figure 6 with depth to top D (2.5 m) and depth extent T (10 m), and assume it is divided into three subplates, each contributing 33% to the surface secondary potential. The depths to the subplate boundaries ($d_i, i = 1, 2$) are found by integrating $1/z$ from D to d_i normalizing this expression by the total contribution of the whole plate (the integral of $1/z$ from D to $D + T$), and equating this result to q_i the percentage surface contribution expressed as a fraction ($0 \leq q_i \leq 1$) giving

$$d_i = D \left(\frac{D+T}{D} \right)^{q_i}, \quad (7)$$

where $q_i = 0.33, 0.67$ for $i = 1, 2$. Other weighting laws such as $1/z^3$ and $1/z^2$ tend to give cells too small close to the top of the plate which produce matrices even larger than those obtained with homogeneous discretizations.

Figure 7a shows the apparent resistivities calculated by vertically dividing the plate into 2, 4, and 8 subplates, and horizontally dividing each subplate into cells with $\Delta y/\Delta z$ ratios close to unity. Long cells with $\Delta y/\Delta z$ ratios greater than two tend to deteriorate the response (the degrading effect on the accuracy of long thin cells has been discussed by Pridmore *et al* (1981) regarding the use of the finite element method in 3-D modeling). Also plotted is the response obtained with a homogeneous grid of 15x15 cells, which is used again to estimate accuracy errors in the responses of the inhomogeneous grids (Figure 7b). The total number of cells, the Δ/d ratios, and the percentage and rms errors are displayed in Table 1 for the cases from 2 to 8 subplates. Significant savings in computer memory and execution time are gained with the weighted discretization. For the case of 8 subplates a maximum error of 0.8% and a 0.4 $\Omega \cdot m$ root mean squared (rms) error were obtained using only 55 cells, in contrast with 225 cells in the 15x15 homogeneous grid. Notice that stronger accuracy criteria for cell discretization are required for this test case compared to those of the horizontal plate. For Δ/d ratios of the order of 1.0 and 0.5, maximum errors of the order of 10% and 5% are obtained.

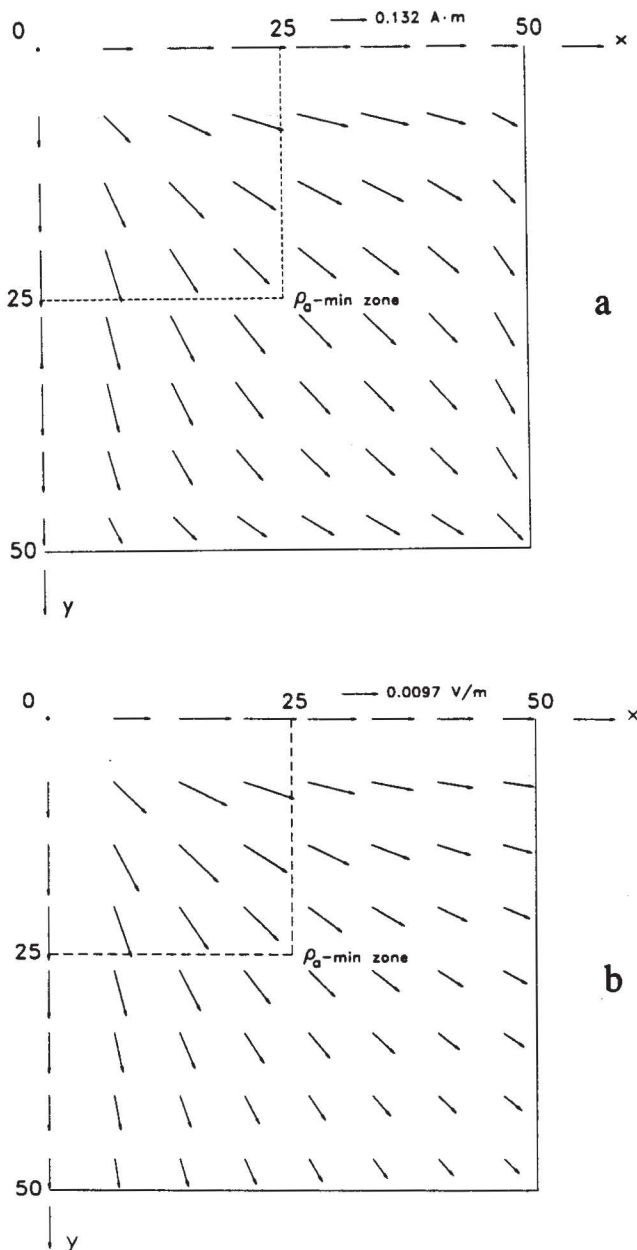


Fig. 3. Spatial configuration of the distributed current dipole moments (a) and the impressed electric fields (b) over the horizontal plate of Figure 2a. Only one quadrant of the plate is shown. The arrows are plotted at the center of each square cell of the 15x15 grid. Injected current is 1 A.

Table 1

Discretization parameters and errors for the vertical plate model

Number of subplates	Number of cells	Δ/d ratio	Max. error (%)	rms error ($\Omega \cdot m$)
2	6	1.24	-12.1	5.7
3	12	0.73	-7.3	3.3
4	21	0.5	-4.8	2.0
5	32	0.38	-2.6	1.0
8	55	0.22	0.8	0.4

The Dipping Plate

This case compares the plate results against two independent solutions to the thin-conductor problem. The model is a 100 by 100 m highly conductive plate (conductance of 5 S) in a $1000 \Omega \cdot m$ homogeneous earth (Figure 8a). Its top is at a depth of 17.5 m and dips 45° . The response is computed along the $y = 0$ axis, assigning the apparent resistivities to the central point of a mobile pair of potential electrodes separated 10 m. The current electrodes are fixed at $(-500,0,0)$ and $(500,0,0)$.

The two curves of Figure 8b were reported by Eskola *et al.* (1989). The solid curve was obtained by these workers using their integrodifferential approach, where the electric charge density was solved in 400 square cells. The dashed curve was calculated with the equipotential solution of Eloranta (1984), valid for thin conductors of high resistivity contrasts. These curves are almost identical because the plate is saturated with current (current channeling number of 50), such that it practically behaves as a perfect conductor.

The squares in Figure 8b are the apparent resistivities derived with the present method, where the plate was divided into 22 subplates comprising a total of 439 cells. This number is comparable with the 400 cells used by Eskola *et al.* Our response closely follows the other two curves but significant discrepancies close to the top of the plate are evident. A maximum absolute error of 8.6% and an rms error of $25.2 \Omega \cdot m$ (2.5% of the host resistivity) are obtained. Although our response converges toward the other two solutions as the number of cells increases, the rate of convergence is slow. This may be explained by the different character of the fields of the two kinds of sources utilized to simulate the current channeling produced by the conductor. Our technique uses the current dipole as fundamental source while Eskola *et al.* utilize the point electric charge. To get a given secondary field at the surface a larger number of dipoles on the plate are required because the field of a dipole decays more rapidly with distance than that of a charge. This is an advantage of the charge density approach over our method. However, it is important to emphasize that this test deals with extreme model parameters, particularly in the large depth extent of the plate compared to its depth of burial, and in the fact that the plate behaves as a perfect conductor in this model. We expect smaller discrepancies for models with geometric and electric parameters not so extreme.

A Solid Body

We examine now the approximation of solid conductive bodies with plates. We show that the plate model not only can be used to represent thin conductive bodies but also can approximate solid inhomogeneities if two or more plates are employed. The testing model is a cube of 2 m sides and resistivity $20 \Omega \cdot m$, located in a half-space of $100 \Omega \cdot m$ at a depth of 0.5 m (Figure 9a). Pridmore *et al.*, (1981) adopted this model to compare the performance of their finite element algorithm with the volume integral equation solution of Hohmann (1975). We have used their

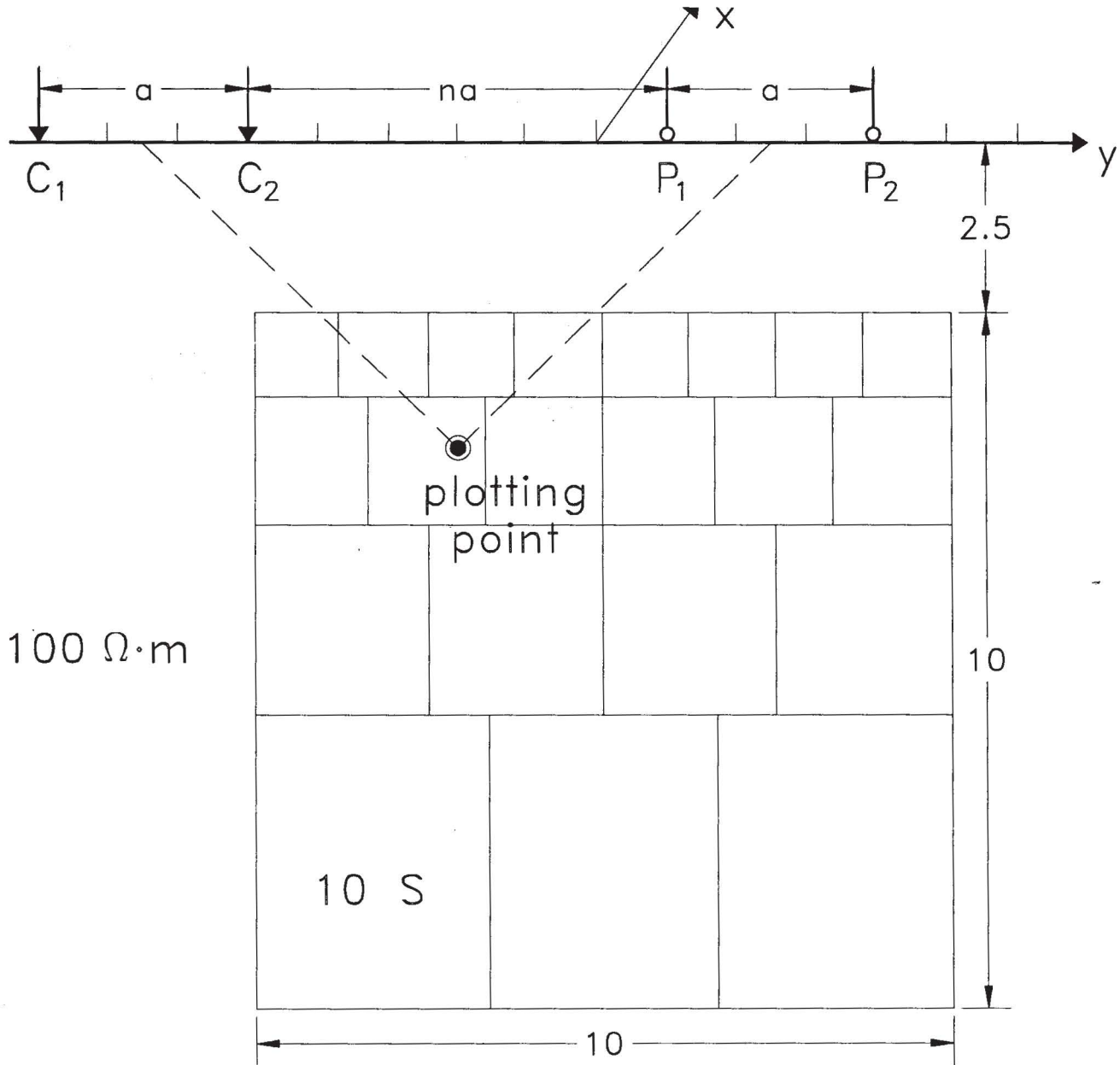


Fig. 4. Model parameters of the vertical plate and location of the dipole-dipole array. A discretization into 4 subplates and 21 cells is displayed. Also shown is one plotting point where the calculated apparent resistivity is assigned.

same dipole-dipole array with $a=1$ m and variable n from 1 to 6 to calculate the apparent resistivities.

There is a variety of ways in which this body can be approximated with plates. However, the set of plates should possess a good geometric coupling with the primary field to obtain accurate results in order to maximize the impressed fields, i.e. the planes of the plates should be as parallel as possible to the primary field set up by the dipole-dipole array. A stack of horizontal plates does not fulfill this requirement, and consequently its response (not shown) has large misfits with the Pridmore and Hohmann results. In contrast, a set of vertical plates parallel to the y -axis more adequately complies with this condition.

Figure 9c shows, in a pseudosection format, how the results of the three methods compare. The multiplate response was calculated with 5 vertical slabs that were located at the center of 5 vertical slabs of equal thickness covering the entire volume of the cube (Figure 9b). A conductance of $0.02 S$ was assigned to each plate, this value being one fifth of the total cube conductance. Each plate was discretized into 4 subplates, considering a total of 100 cells. A good agreement between the multiplate response and the other two results is apparent; rms errors of 3.9 and $2.9 \Omega \cdot m$ result between the plate response and the finite element and integral equation values, respectively. These errors are comparable with the $2.7 \Omega \cdot m$ rms error between the Pridmore and Hohmann results. However, a maximum

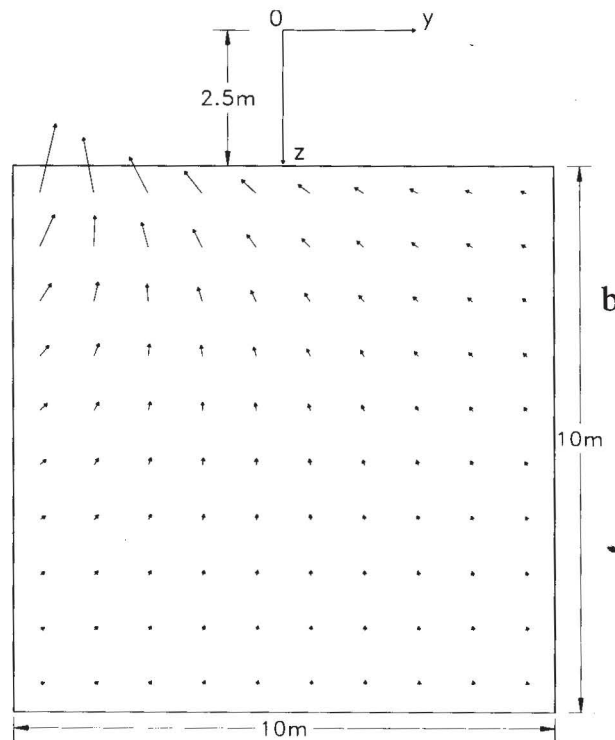
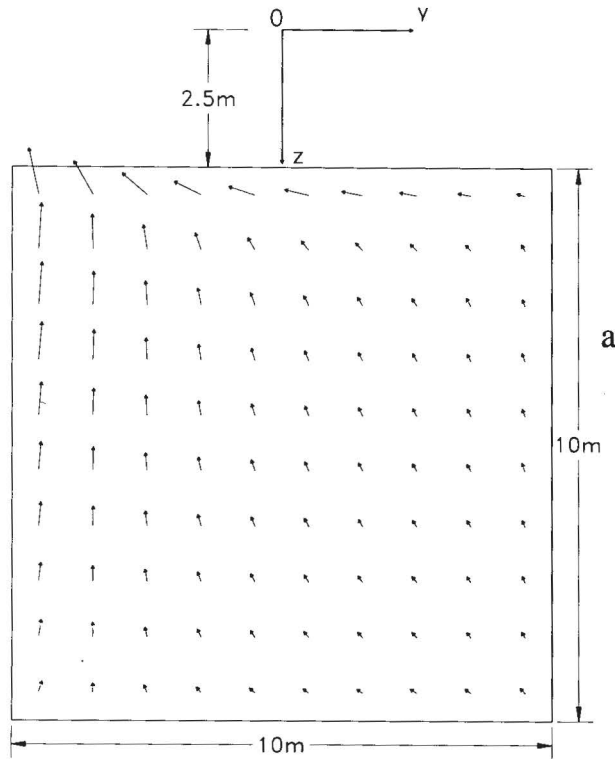


Fig. 5. Moments of the distributed current dipoles (a) and the impressed electric fields (b) over the vertical plate model of Figure 4 for an injected current of 1 A. Current electrodes at (-8,0,0) and (-5,0,0). The arrows are plotted at the center of each square cell for a 15x15 homogeneous discretization.

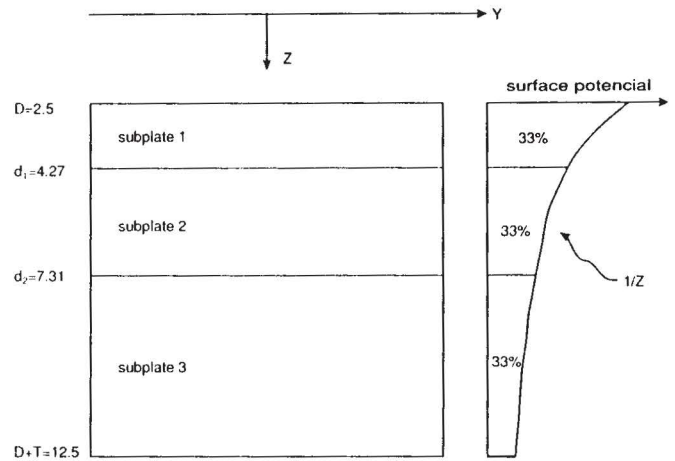


Fig. 6. Example of a division of the plate of Figure 4 into 3 subplates using the proposed weighted vertical discretization. Each subplate contributes 33% to the surface secondary potential (in arbitrary units).

error of 17.7% is obtained between the plate results and the other two techniques, which is significantly larger than the corresponding 6.6% maximum error between the finite element and the integral equation results. Increasing the number of vertical plates does not significantly reduce the 17.7% maximum error.

A Solid Body in a Two-Layered Host

This case illustrates the approximation of a rectangular prism when the surrounding medium is a two-layered earth. Figure 10 shows the brick model utilized by Das and Parasnis (1987) to compare the response of their surface integral equation solution against that of a finite differences algorithm (Dey and Morrison, 1979). We approximated the brick with five vertical plates parallel to the y-axis, in a similar fashion as done for the cubic model. Each plate was vertically divided into 5 subplates, utilizing a total of 80 cells. The results calculated with 60 image terms for a dipole-dipole array ($n=1, 3, \text{ and } 7$) are shown in Figure 10b together with the apparent resistivities computed from the other two techniques. A good agreement between the responses is evident. Absolute maximum errors and rms errors of the plate response with the surface integral equation and the finite differences responses are 4.2% and $0.9 \Omega \cdot m$, and 9.1% and $1.25 \Omega \cdot m$, respectively. These magnitudes are comparable with those between the other two techniques (5.2% and $0.7 \Omega \cdot m$).

CONCLUSIONS

We have tested, with five different models, the performance of an integral equation algorithm that computes the apparent resistivity response of one or several conductive plates. In the first two cases we demonstrated internal convergence with increasing discretization, whereas in each of the next three cases we compared the plate response with two independent numerical solutions previously reported in the literature.

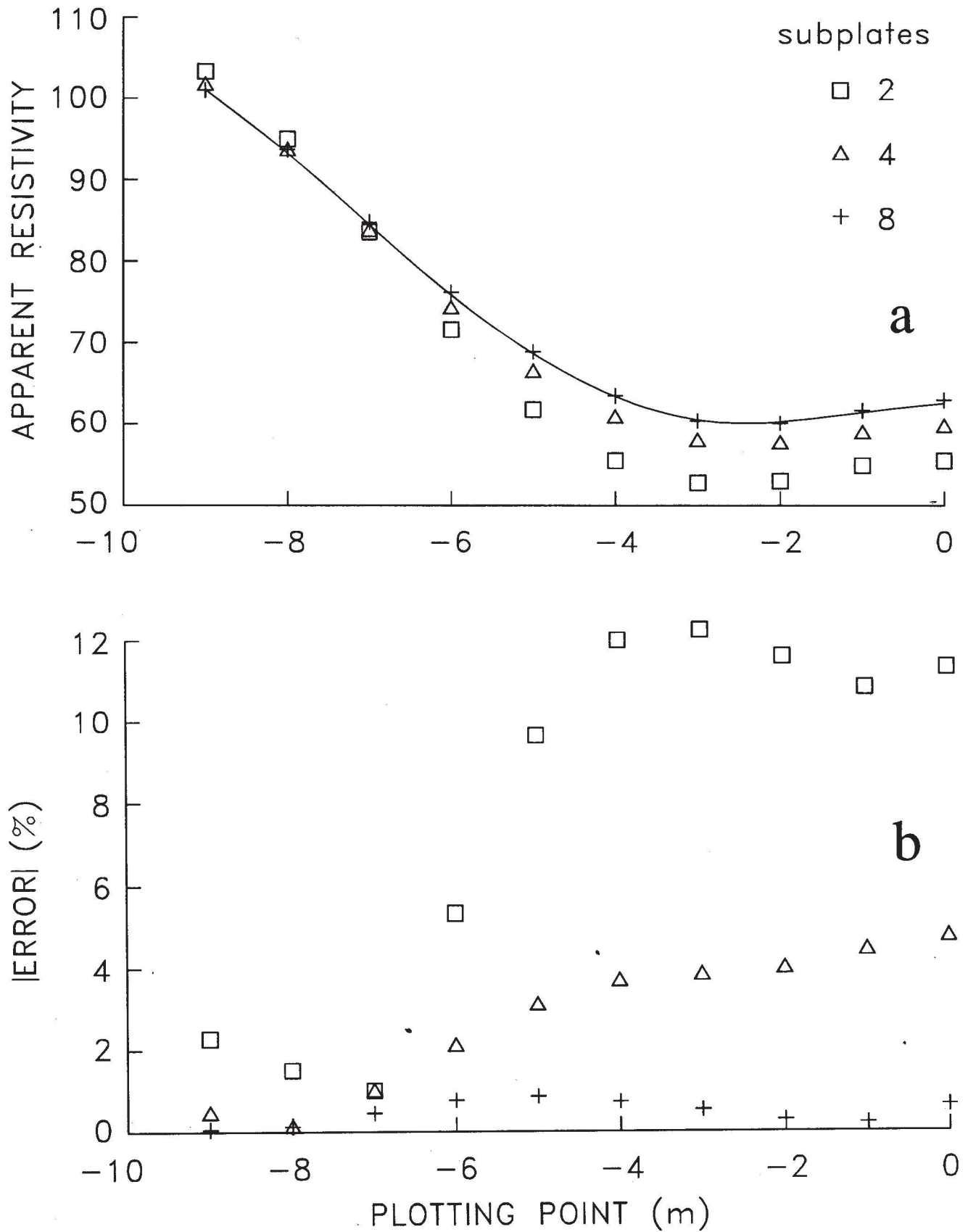


Fig. 7. a) Comparison of apparent resistivities from different discretizations of the vertical plate model. b) Absolute errors of the three different heterogeneous discretizations (2,4, and 8 subplates) with respect to the 15x15 grid.

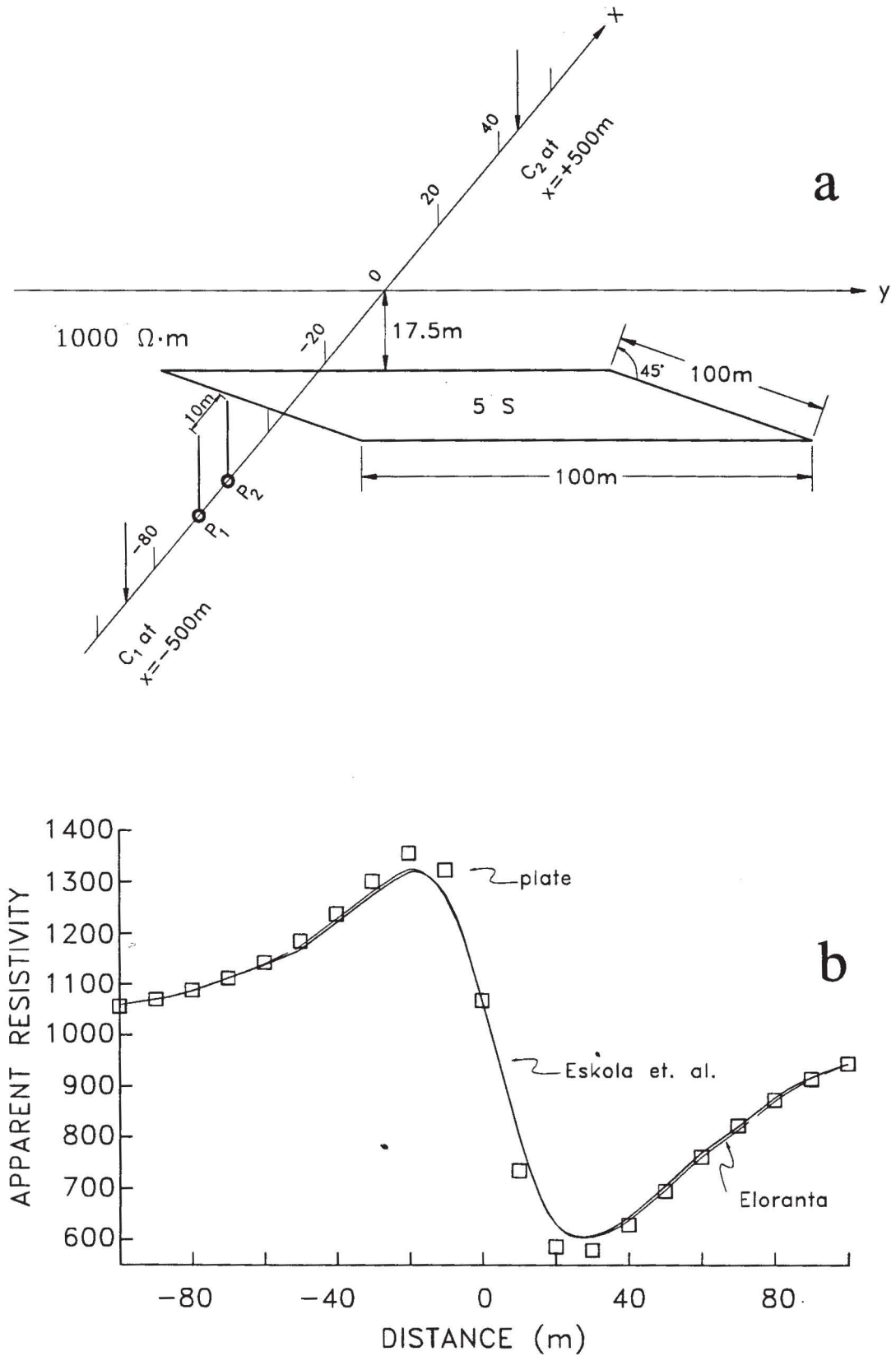


Fig. 8. a) The dipping conductor model of Eskola *et al.*, (1989) and location of the electrode array. b) Comparison of apparent resistivity responses: squares, present method; solid line, integrordifferential solution of Eskola *et al.*; dashed line, equipotential results using the method of Eloranta (1984).

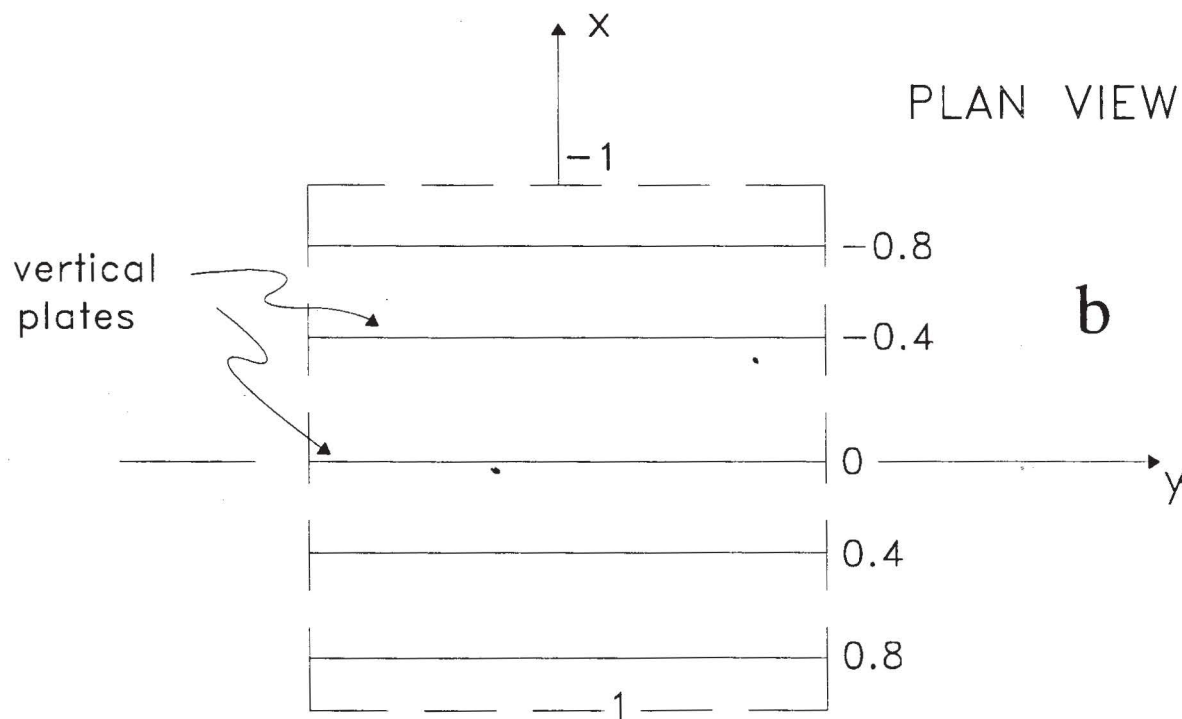
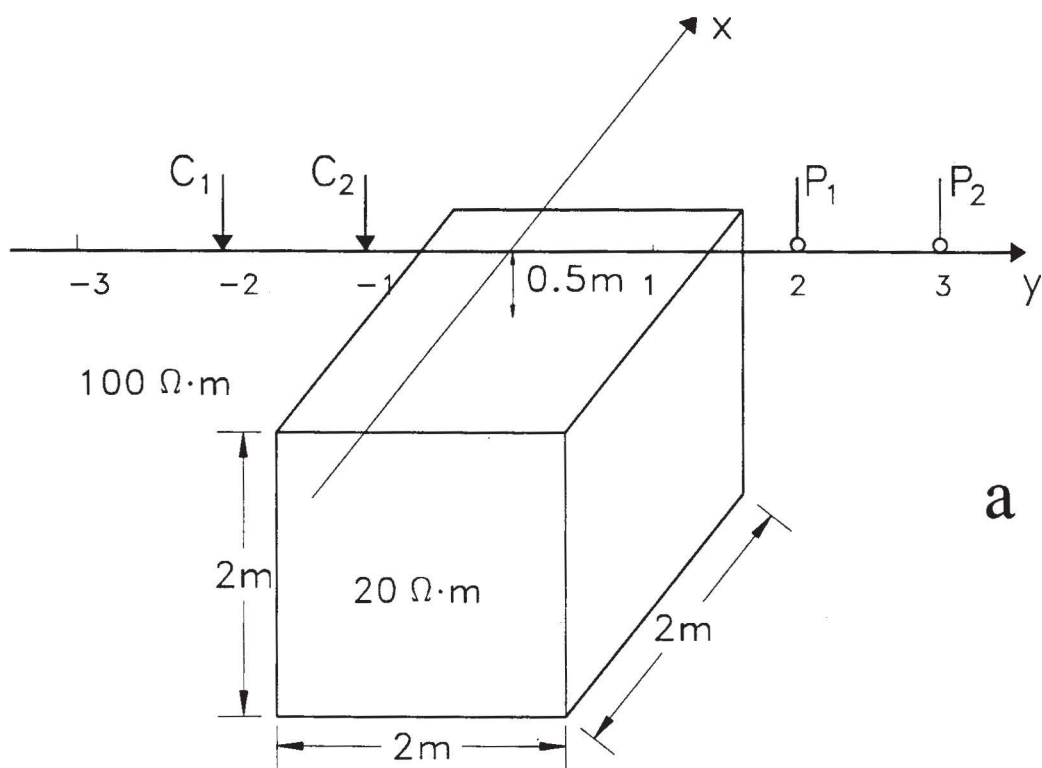


Fig. 9. a) The cube model of Pridmore *et al.*, (1981) and location of the dipole-dipole profile. b) Plan view showing the approximation of the body with five vertical plates. c) Comparison of apparent resistivity pseudosections from the plate, finite element, and volume integral equation algorithms.

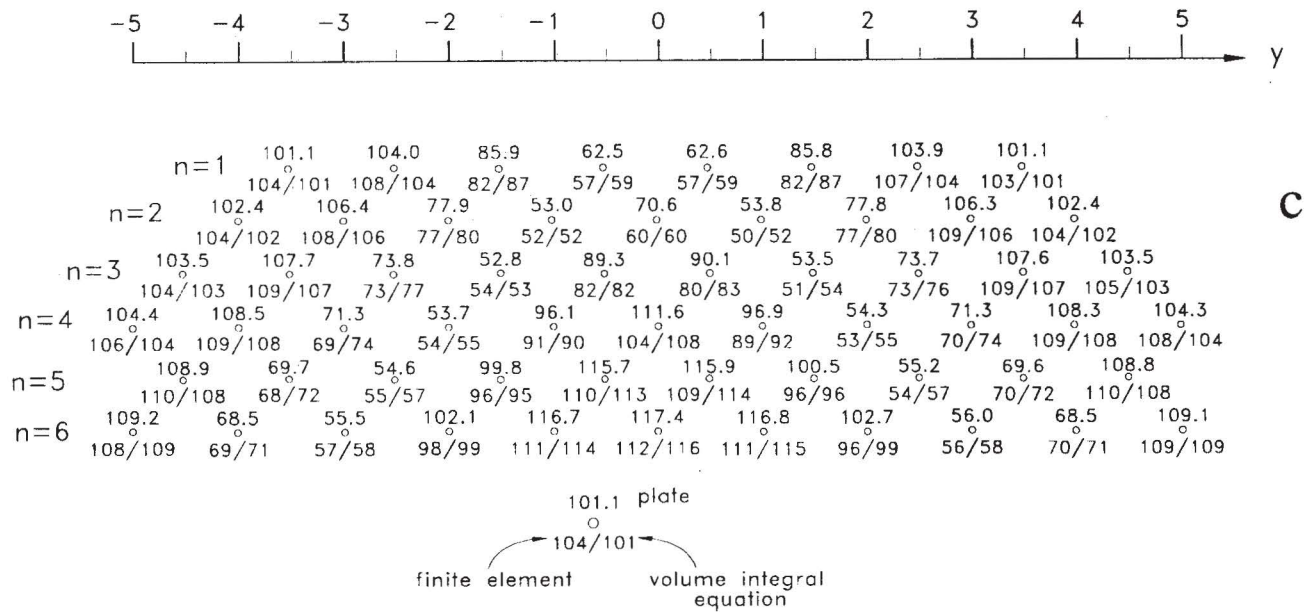


Fig. 9. (Cont.).

The horizontal plate model illustrates that the geometric coupling existing between the plate and the primary electric field has an important effect on the calculated response. The current saturation approach of Nabighian *et al.*, (1984), besides providing a good physical insight to the problem, permits the a priori adoption of a fine or a gross discretization by simply examining the current channeling number of the anomalous body. Both the horizontal and vertical plate models were analyzed using highly conducting plates with corresponding high current channeling numbers, such that the proposed Δ/d discretization ratios are adequate for situations where the plate gathers current in the current saturation regime. For plates with lower current channeling numbers the Δ/d ratios can be relaxed to obtain the same accuracy levels. Important savings in computer memory and execution time are gained with the use of the weighted vertical discretization illustrated in the vertical plate model. This discretization approach can also be applied to other surface or volume integral equation algorithms.

For the dipping conductor model the plate results were compared with the numerical solutions of Eskola *et al.*, (1989) and Eloranta (1984), which we assumed as true converging values based on the close agreement of their apparent resistivities. If this assumption is valid, this case would show that the charge density approach of Eskola *et al.*, is more accurate than our current dipole scheme, likely due to the slower decaying behavior of the field of a charge as compared to that of a dipole; our response shows overshooting and undershooting over the apparent resistivity maximum and minimum, respectively, characteristic of a dipolar field. Despite this shortcoming, this test can be considered satisfactory given the small rms error (2.5% of the host resistivity). Both methods are comparable in terms of flexibility and computer time.

The simulation of solid conductive bodies with a set of vertical plates is satisfactory but certainly not optimum, specially for the cubic body in a homogeneous earth. The large errors (less than 20%) in some apparent resistivities right over the plates could not be significantly decreased even by increasing the number of plates or by using a finer cell discretization. We suspect these inaccuracies are still due to a non-optimum geometric coupling; so far we have not found a better option other than the vertical plate arrangement.

The flexibility of the multiple plate technique promises to be a useful tool not only in the actual interpretation of resistivity studies but also in survey design and in the analysis of the perturbing effect of shallow inhomogeneities in multiple conductor settings.

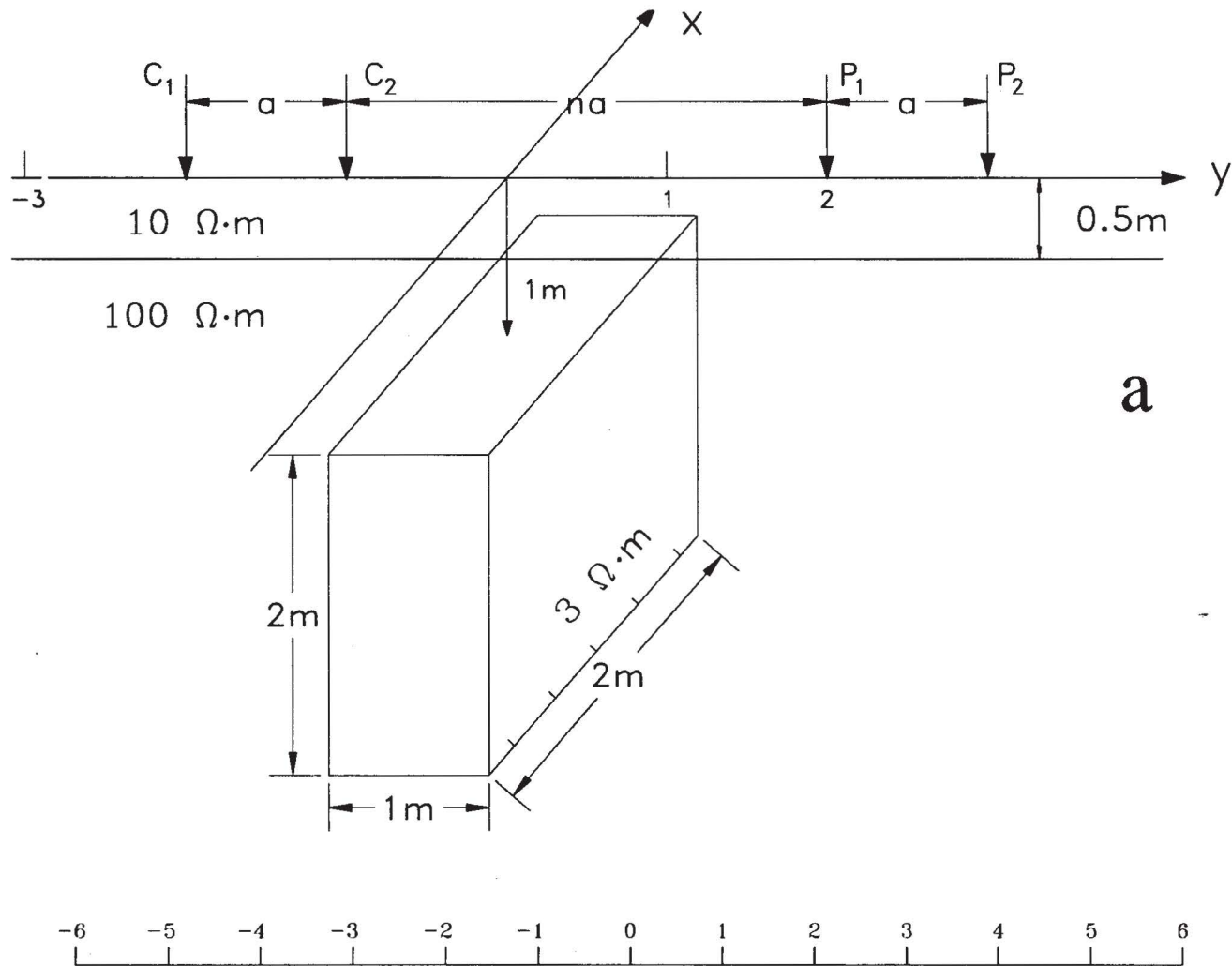
ACKNOWLEDGMENTS

We thank Paulo González and Dolores Carvajal for their assistance. One of the authors (C.B.) was supported during the course of this research by scholarships from CONACYT and CICESE. The project was financed by a grant from CICESE.

APPENDIX.

Derivation of the Image Terms for a Two-Layered Earth

Consider a two-layered half-space defined by the resistivities ρ_1 , ρ_2 , and the thickness t of the first layer. The bases for the expansion into images of the electric potential at (x, y, z) produced by a point current source I at (x', y', z') can be found in several standard texts (e.g. Orellana, 1972). There are two sets of expressions for the potential depending on where the current source is located. When the source is in layer 1, suitable solutions are



n=1	16.6	16.6	16.6	16.7	16.6	16.3	16.4	16.6	16.6	16.6	16.6	16.6	16.6
	16.6	16.6	16.7	16.7	16.7	16.2	16.2	16.7	16.7	16.7	16.7	16.6	16.6
	16.7	16.5	16.6	16.5	16.6	16.1	15.6	16.1	16.7	16.7	16.7	16.5	16.7
n=3		32.7	32.8	32.4	31.3	31.6	32.0	31.7	32.2	32.7	32.7	32.7	
		32.8	33.1	32.7	30.9	30.5	30.7	30.9	32.7	32.8	32.8		
		33.7	33.5	33.5	31.9	29.3	29.1	29.4	31.3	33.7	34.0		
n=7				52.3	53.4	53.8	53.9	53.8	53.3	plate			
				50.8	51.5	51.8	51.9	52.2	52.3	surface integral equation			
				50.9	51.4	51.8	52.1	52.1	52.0	finite differences			

Fig. 10. The conductive brick model in a two-layered earth. a) Model geometry and location of the dipole-dipole array. b) Comparison of apparent resistivities from the present method, the surface integral equation approach of Das and Parasnis (1987) and the finite differences formulation of Dey and Morrison (1979).

$$V_{1,1}(r, z) = \int_0^{\infty} \left[A_1 e^{-\lambda z} + A_2 e^{\lambda z} + \frac{\rho_1 I}{4\pi} e^{\lambda(z-z')} \right] J_0(\lambda r) d\lambda, \quad \text{for } z \leq z';$$

$$V_{1,1}(r, z) = \int_0^{\infty} \left[A_1 e^{-\lambda z} + A_2 e^{\lambda z} + \frac{\rho_1 I}{4\pi} e^{\lambda(z'-z)} \right] J_0(\lambda r) d\lambda, \quad \text{or } z' \leq z \leq t;$$

$$V_{1,2}(r, z) = \int_0^{\infty} A_3 e^{-\lambda z} J_0(\lambda r) d\lambda, \quad \text{for } z \leq t;$$

where $r^2 = (x-x')^2 + (y-y')^2$, the first and second subscripts of V indicate in which layer are located the source and field points, respectively, and $J_0(\cdot)$ is the Bessel function of the first kind and order zero.

The corresponding potentials when the source is in layer 2 are

$$V_{2,1}(r, z) = \int_0^{\infty} [B_1 e^{-\lambda z} + B_2 e^{\lambda z}] J_0(\lambda r) d\lambda, \quad \text{for } 0 \leq z \leq t;$$

$$V_{2,2}(r, z) = \int_0^{\infty} \left[B_3 e^{-\lambda z} + \frac{\rho_2 I}{4\pi} e^{\lambda(z-z')} \right] J_0(\lambda r) d\lambda, \quad \text{for } t \leq z \leq z';$$

$$V_{2,2}(r, z) = \int_0^{\infty} \left[B_3 e^{-\lambda z} + \frac{\rho_2 I}{4\pi} e^{-\lambda(z-z')} \right] J_0(\lambda r) d\lambda, \quad \text{for } z' \leq z.$$

The arbitrary constants A_i, B_i are determined from the boundary conditions that the potential and the vertical component of the current density must be continuous across $z=t$, and that there is no vertical component of the current density at $z=0$. The integral

$$\int_0^{\infty} e^{-\lambda z} J_0(\lambda r) d\lambda = \frac{1}{(r^2 + z^2)^{1/2}}$$

is used to integrate the expressions for V term-by-term having first expanded the denominator by the binomial theorem. The resulting expressions for the potentials in terms of an infinite sum of images are

$$\begin{aligned} V_{1,1} &= \frac{\rho_1 I}{4\pi} \left[\frac{1}{[r^2 + (z-z')^2]^{1/2}} + \frac{1}{[r^2 + (z+z')^2]^{1/2}} + \right. \\ &\quad \left. \sum_{n=1}^{\infty} K_{21}^n \left\{ \frac{1}{[r^2 + (z+z'-2nt)^2]^{1/2}} + \frac{1}{[r^2 + (z-z'-2nt)^2]^{1/2}} + \right. \right. \\ &\quad \left. \left. \frac{1}{[r^2 + (z-z'+2nt)^2]^{1/2}} + \frac{1}{[r^2 + (z+z'+2nt)^2]^{1/2}} \right\} \right] \\ V_{1,2} &= \frac{\rho_2 I}{4\pi} \left[(1-K_{21}) \sum_{n=0}^{\infty} K_{21}^n \left\{ \frac{1}{[r^2 + (z-z'+2nt)^2]^{1/2}} + \right. \right. \\ &\quad \left. \left. \frac{1}{[r^2 + (z+z'+2nt)^2]^{1/2}} \right\} \right], \\ V_{2,1} &= \frac{\rho_2(1-K_{21})I}{4\pi} \sum_{n=0}^{\infty} K_{21}^n \left\{ \frac{1}{[r^2 + (z-z'-2nt)^2]^{1/2}} + \right. \end{aligned}$$

$$\left. \frac{1}{[r^2 + (z+z'+2nt)^2]^{1/2}} \right\},$$

$$\begin{aligned} V_{2,2} &= \frac{\rho_2 I}{4\pi} \left\{ \frac{1}{[r^2 + (z-z')^2]^{1/2}} + \frac{(1-K_{21}^n)}{[r^2 + (z+z')^2]^{1/2}} + \right. \\ &\quad \left. \frac{-K_{21}}{[r^2 + (z+z'-2t)^2]^{1/2}} + (1-K_{21}^n) \sum_{n=1}^{\infty} \frac{K_{21}^n}{[r^2 + (z+z'+2nt)^2]^{1/2}} \right\}, \end{aligned}$$

where K_{21} is the reflection coefficient $(\rho_2 - \rho_1) / (\rho_2 + \rho_1)$. These are the expansions for the potentials produced by point sources. The corresponding expressions for the potentials due to distributed current dipoles are derived by differentiation with respect to the dipole direction and integration over the cell area. The corresponding primary electric fields only require differentiating the point potentials with respect to the required field component, while the Green's functions need a differentiation in the direction of the field component, another differentiation in the direction of the current dipole, and a final double integration over the cell area.

BIBLIOGRAPHY

- BARAJAS, C., 1989. Cálculo de la respuesta en resistividad de cuerpos conductores en un medio estratificado. M. Sc. Thesis, CICESE.
- CHEESMAN, S. J. and R. N. EDWARDS, 1989. Current channelling in square plates with applications to magnetometric resistivity. *Geophysical Prospecting*, 37, 553-581.
- DAS, U. C. and D. S. PARASNIS, 1987. Resistivity and induced polarization responses of arbitrarily shaped 3-D bodies in a two-layered earth. *Geophysical Prospecting*, 35, 98-109.
- DEY, A. and H. F. MORRISON, 1979. Resistivity modeling for arbitrarily shaped three-dimensional structures. *Geophysics*, 44, 753-780.
- DIETER, K., N. R. PATERSON and F. S. GRANT, 1969. IP and resistivity type curves for three-dimensional bodies. *Geophysics*, 34, 615-632.
- ELORANTA, E., 1984. A method for calculating mise-à-la-masse anomalies in the case of high conductivity contrast by the integral equation technique. *Geoexploration*, 22, 77-88.
- ESKOLA, L., H. SOININEN and M. OKSAMA, 1989. Modelling of resistivity and IP anomalies of a thin conductor with an integral equation. *Geoexploration*, 26, 95-104.
- FLORES, C. and R. N. EDWARDS, 1992. Approximate calculation of low-frequency three-dimensional magnetotelluric responses using a multiple plate model. *Geophysics*, 57, 106-115.

GRANT, F. S. and G. F. WEST, 1965. Interpretation theory in applied geophysics, McGraw Hill Book Co.

HOHMANN, G. W. 1975. Three-dimensional induced polarization and electromagnetic modelling. *Geophysics*, 40, 309-324.

NABIGHIAN, M. N., G. L. OPPLIGER, R. N. EDWARDS, B. B. H. LO and S. J. CHEESMAN, 1984. Cross-hole magnetometric resistivity (MMR). *Geophysics*, 49, 1313-1326.

OKABE, M., 1981. Boundary element method for the arbitrary inhomogeneities problem in electrical prospecting. *Geophysical Prospecting*, 29, 39-59.

ORELLANA, E., 1972. Prospección geoeléctrica en corriente continua, Paraninfo, Madrid.

PRIDMORE, D. F., G. W. HOHMANN, S. H. WARD and W. R. SILL, 1981. An investigation of finite-element modeling for electrical and electromagnetic data in three dimensions. *Geophysics*, 46, 1009-1024.

César Barajas¹ and Carlos Flores

Depto. de Geofísica Aplicada, CICESE. Tijuana-Ensenada, km. 107 Carretera Tijuana-Ensenada, Ensenada, Baja California, México.

¹ Presently at: Institut für Geophysik, Christian-Albrechts-Universität Kiel, Olshausenstr. 40-60, 2300 Kiel 1, Fed. Rep. of Germany